RSC Advances

ROYAL SOCIETY OF CHEMISTRY

www.rsc.org/advances

Journal Name

RSCPublishing

ARTICLE

Site occupations of Zn in $AgInSe_2$-based chalcopyrites responsible for modified structures and significantly improved thermoelectric performance

Li Wang, Penzhan Ying, Yuan Deng, Hong Zhou, Zhengliang Du, and Jiaolin Cui*

Cite this: DOI: 10.1039/xOxxOOOOOx

Received OOth January 2012,
Accepted OOth January 2012

DOI: 10.1039/xOxxOOOOOx

www.rsc.org/

The band structures of $AgInSe_2$-based semiconductors have been calculated and the lifting of Fermi level toward the conduction band in $AgInSe_2$ when Ag is replaced by Zn has been observed. This is mainly caused by the site occupation of Zn on the cation Ag site, which leads to the formation of the defect Zn^{+1}_{Ag} as an active donor. While the Fermi level lowers toward the valence band when In is replaced by Zn, due to the primarily formation of an acceptor Zn^{-1}_{In}. The ZT value reaches 0.95±0.10 at ~815K through substituting Zn for Ag and In simultaneously. However, a higher ZT value of 1.05±0.12 has been achieved by substituting a proper amount of Zn for Ag through largely enhancing the carrier concentration n and reducing the lattice thermal conductivity via modifying the crystal structure. Hence, we propose that when Ag is replaced by Zn in $AgInSe_2$ there are at least two factors i.e. the carrier concentration n and bandgap E_g that govern the electrical property, and that the enhancement in carrier concentration n seems to have a more prominent effect than the widening of bandgap E_g does.

1. Introduction

Developing high performance thermoelectric (TE) materials is currently a heated topic of discussion. The TE performance is directly related to the dimensionless figure of merit ZT, $ZT=T\alpha^2\sigma/\kappa$, where T is absolute temperature, α is the Seebeck coefficient, σ is the electrical conductivity and κ is the thermal conductivity consisting of electronic (κ_e) and lattice (κ_L) components. In order to develop the materials with high TE performance, several successful strategies have been proposed, such as the modification of the electron states with resonant impurities,[1-3] engineering band convergence,[4,5] nanostructures,[6,7] strong electron–phonon coupling by charging density waves,[8] and liquid–like thermoelectrics.[9] However, the ZT values are still limited to around unity in current commercial materials.[10]

$AgInSe_2$ (AIS) is a kind of I–III–VI_2 semiconducting compounds crystallizing in a chalcopyrite structure. Similar to other ternary chalcopyrite–structured compounds, there is an inherent Coulomb attraction between charged defects In^{2+}_{Ag} and $2V^{-1}_{Ag}$ (a native defect pair, i.e., metal In–on–Ag anti-sites and two Ag vacancies) in AIS. Because of the partial annihilation on the corresponding acceptor and donor levels in this defect pair, the carrier concentration n is rather low (n=10^{22}~$10^{23}$$m^{-3}$ at room temperature),[11–13] which is one of the key factors that degrades the ZT value (ZT=0.34 at 724K).[14] However, the carrier concentration n can be enhanced via proper element substitution, for example, Zn and Ge codoping in $CuGaSe_2$ can increase the concentration of shallow donor levels, leading to the formation of a higher density of electrically active donors Zn_{Cu} and resulting in n–type conduction.[15] Upon the addition of Zn in AIS, we believe that the element Zn occupies the cation (In or Ag) sites, rather than anion (Se) sites, because of the relatively small electronegativity of Zn (1.65) compared to those of In (1.78) or Ag (1.93). In this case, we anticipate a primarily formation of the monovalence Zn^{+1}_{Ag} or Zn^{-1}_{In} defect that acts as an active donor or acceptor respectively.

In addition, the action of Zn in AIS has a profound effect on the crystal and band structures. Upon the occupations of Zn in AIS lattice sites, not only can we expect the complicated anion (Se) displacement in the crystal structure due to larger electronegativity difference between cation Zn and anion Se, but also the widening of the energy gap (E_g) due to increased ionicity in this material.[16] The additional hybridization of Zn $3d^{10}$ with Se $4p^4$ orbitals will enable the chalcopyrite lattice to dilate (compress), which makes the cation–anion distance increase (decrease) and the p–d admixture reduce (enhance). As a result, the E_g value increases (decreases).[17] Hence Zn is an element that can effectively manipulate the electronic

structure and carrier concentration.[18] It can thus tailor the TE performance just like the element Sb does in $CuGaTe_2$.[19]

In this work, we calculated the band structures upon the substitutions of Zn for Ag and In respectively, and observed a lifting (lowering) of the Fermi level toward the conduction (valence) band because of the primarily formation of Zn^{+1}_{Ag} (Zn^{-1}_{In}) as Zn occupies in the Ag (In) lattice sites, as well as a remarkable change in TE performance. The maximum *ZT* value of 1.05±0.12, which is about 3 times that of the intrinsic AIS, was obtained in $Ag_{1-x}InZn_xSe_2$ (x=0.1) at 815 K.

2. Results and Discussion

2.1. X-ray Diffraction Patterns and EPMA Analysis

The x–ray diffraction patterns of $Ag_{1-x}In_{1-x}Zn_{2x}Se_2$ (labeled as IA–poor) and $Ag_{1-x}InZn_xSe_2$ (labeled as Ag–poor) powders indicate that both the Ag–poor and IA–poor samples crystallize in a single $AgInSe_2$ phase (PDF 75–0118) until x=0.1, as shown in **Fig.S1 a** and **b**. In two sorts of the materials at x=0.1, a minor impurity phase $Zn_{0.4}In_2Se_{3.4}$ (PDF 40–0912) was identified, suggesting that an increase of Zn content (x≥0.1) in AIS helps to form the Zn–containing compounds. We therefore stop the investigations of the materials that contain x> 0.1 Zn contents.

The chemical compositions for AIS, Ag–poor and IA–poor (x=0.1) each taken from a mapping of EPMA are shown **Table S1**, and a mapping picture of $Ag_{1-x}In_{1-x}Zn_{2x}Se_2$ (x=0.1) in the **Fig.S2.** In **Table S1** we observed that the relative molars of Ag, In, Zn and Se identified are close to those of as–prepared materials, except for a little deficiency in Se and excess in In. The results suggest that the Zn composition is almost as intended in the final samples.

2.2 Structure Analyses

2.2.1 Band Structure Calculations

We calculated the band structures of Zn–doped AIS near the band gap regions. Basically, Zn occupies in the AIS lattice sites in two ways, which are the occupations on Ag and In site. Therefore, the three arrangements of Zn on Ag, In and both lattice sites, each of which corresponds to the chemical formulas of $Ag_{0.5}InZn_{0.5}Se_2$, $AgIn_{0.5}Zn_{0.5}Se_2$ and $Ag_{0.5}In_{0.5}ZnSe_2$, are the focus of this calculation.

The calculated band structure of AIS is plotted in **Fig.1a**, where a direct band gap was observed, with the valence band maximum (VBM) and conduction band minimum (CBM) both located at the Γ point. The Fermi level is at the top of the valence band. The calculated bandgap (E_g) of AIS is ~0.71eV, which is smaller than the reported value (1.18~1.22eV).[11,16] The calculated E_g value is lower than what is expected due to the well–known Local Density Approximation (LDA)/GGA problem.

The AIS with 50% Zn on the In sites (the material $AgIn_{1-x}Zn_xSe_2$ (x=0.5) with this arrangement is labeled as In–poor) reveals that the Fermi level lies in the valence band with a direct bandgap of ~0.7eV (shown in **Fig.1b**). The drop of Fermi level to the valence band implies that the group II atom (Zn) is an acceptor on the group III (In) site. In contrast to the band structure of In–poor sample, we observed that the Fermi level moves to the conduction band in Ag–poor sample (x=0.5) with the direct bandgap reaching ~0.73eV (**Fig.1c**). However, the band structure almost does not change in IA–poor sample (x=0.5) with the Fermi level still lying on the top of the valence band, which is similar to that in intrinsic AIS (see **Fig.1d**). The change of the band structure upon element substitutions suggests that the occupation of Zn for Ag (or for In) sites form the antisite defect Zn^{+1}_{Ag} (or Zn^{-1}_{In}), which play a dominant role in yielding the "lowering" (or "lifting") of both the CBM and VBM simultaneously. Although there is a chance to have another two defects involving intrinsic In^{2+}_{Ag} and V^{-1}_{Ag} when Zn occupies the Ag sites, the effect of V^{-1}_{Ag} as an acceptor on the band structure has been neutralized by Zn^{+1}_{Ag} as a donor. On the other hand, the defect Zn^{+1}_{Ag} is possible to appear in addition to Zn^{-1}_{In} upon the substitution of Zn for In, due to the preoccupation of Zn on the Ag sites, similar to the case of Mn–substituted $CuInSe_2$.[20] Likewise, it is the action of the acceptor Zn^{-1}_{In} that plays a dominant role in moving the Fermi level (E_F) into the acceptor level.[21] In the partial density of states (DOS) (**Fig.S3**) we observed that Zn–*d* states, mostly lying in the relatively deep level (~7.0eV) in the valence band, do not hybridize with Ag, In and Se states directly. We thereby propose that when Zn occupies the Ag (or In) sites it is the donor (or acceptor) action of Zn^{+1}_{Ag} (or Zn^{-1}_{In}) that lifts (or lowers) the Fermi level into the conduction (or valence) band.

2.2.2 XRPD and Rietveld Refinement

In order to confirm the primarily formation of the defects Zn^{+1}_{Ag} and Zn^{-1}_{In} as Zn substitutes for Ag and In simultaneously, we have calculated the site occupations of Zn ion in In–poor, Ag–poor and IA–poor systems using Rietveld refinement. In chalcopyrite–type $AgInSe_2$, there are two cation sites, Ag on site 4*a* (0, 0, 0), In on site 4*b* (0, 0, 0.5) and Se atoms on site 8*d* (x_{Se}, 0.25, 0.125 with x_{Se}~0.25) coordinated by two Ag and two In cations. The unit cell and structural parameters *a*, *c* and V, x_{Se}, U_{iso} and site occupation factors (SOFs), are required to describe the crystal structure of unsubstituted and Zn–substituted $AgInSe_2$.

The Rietveld refinement results of unsubstituted AIS are illustrated in **Fig.S4** and **Table S2**. The SOFs (0.9522(2), 0.9956(3) and 0.9720(4)) attained suggest that most Ag, In and Se atoms occupy the 4*a*, 4*b* and 8*d* sites with a little position displacement of Se atoms (x_{Se} = 0.2374(3)).

In the refinement of the XRPD experiments of Ag–, In– and IA–poor samples (x=0.025, 0.05), an equal "opportunity" of the Zn ions to occupy both Ag and In cation sites was assumed, and therefore models A (Ag, In, Zn)$_{4a}$(Ag, In, Zn)$_{4b}$(Se$_{2-\delta}$)$_{8d}$, model B (Ag, Zn)$_{4a}$(Ag, In, Zn)$_{4b}$(Se$_{2-\delta}$)$_{8d}$ and model C (Ag, In, Zn)$_{4a}$(In, Zn)$_{4b}$(Se$_{2-\delta}$)$_{8d}$, in which the Se anions exclusively occupy the 8*d* site,

were proposed. In model A the cation sites (4*a* and 4*b*) are proposed to be occupied by Ag, Zn, and In ions simultaneously, while in model B the 4*a* sites are occupied only by Ag and Zn ions, and in model C 4*b* sites only by In and Zn ions, that is,

for model A,

$$SOF(Ag)_{4a} + SOF(Zn)_{4a} + SOF(In)_{4a} = 1 \quad (1)$$
$$SOF(Ag)_{4b} + SOF(Zn)_{4b} + SOF(In)_{4b} = 1 \quad (2)$$
$$SOF(Zn)_{4a} + SOF(Zn)_{4b} = 0.025, 0.05 \text{ and } 0.1 \quad (3)$$

for model B,

$$SOF(Ag)_{4a} + SOF(Zn)_{4a} = 1 \quad (4)$$
$$SOF(Ag)_{4b} + SOF(Zn)_{4b} + SOF(In)_{4b} = 1 \quad (5)$$
$$SOF(Zn)_{4a} + SOF(Zn)_{4b} = 0.025, 0.05 \text{ and } 0.1 \quad (6)$$

for model C,

$$SOF(Ag)_{4a} + SOF(Zn)_{4a} + SOF(In)_{4a} = 1 \quad (7)$$
$$SOF(Zn)_{4b} + SOF(In)_{4b} = 1 \quad (8)$$
$$SOF(Zn)_{4a} + SOF(Zn)_{4b} = 0.025, 0.05 \text{ and } 0.1 \quad (9)$$

Based on the above assumptions and proposals, we attained the finalized structural parameters in three sorts of samples, which are shown in **Table 1** and **Fig.S5.** The fitting rsults using model B and C are shown in **Table S3,4**. From the refinement results, we did not observe visible site preference of Zn in cation sites. For example, the $SOF(Zn)_{4a}$ and $SOF(Zn)_{4b}$ in x=0.025 are 0.0252(2) and 0.0245(3) in model A, 0.0277(4) and 0.0233(7) in model B, and 0.0244(5) and 0.0256(4) in model C, even though there is a little difference between $SOF(Zn)_{4a}$ and $SOF(Zn)_{4b}$ in the same model at x=0.05. Besides, most Ag, In and Se atoms occupy the 4*a*, 4*b*, 8*d* sites, irrelevant to the models proposed. Because the $SOF(Zn)_{4b}$ in In–poor and $SOF(Zn)_{4a}$ in Ag–poor samples are all about 0.05, and the $SOF(Zn)_{4a}$ in In–poor and $SOF(Zn)_{4b}$ in Ag–poor samples are close to 0. Therefore, we come to the conclusion that there is almost no site preference tendency of Zn in the cation sites.

The lattice parameters attained using the parameters shown in **Table 1** are presented in **Fig.2a and b**, and an almost linear decrease of the lattice constants a, c and volume V have been observed with the Zn content increasing in both IA–poor and Ag–poor samples, which might be due to the decrease of the effective cation radius r_{eff}, caused by an increase in total number of cation positions.[22] The relationship between the lattice constants and Zn content (x) follows Vegard's low, which suggests that Zn is incorporated into the crystal lattice in AIS. However, we can not rule out the possibility of the existence of interstitial Zn, Zn_i, in the host cell. In order to confirm that most Zn atoms occupy the cation sites, we analysed the mean cation–Se distance $d_{C–Se}$, and found that the determined $d_{(Ag–Se)4a}$ elongates linearly from 2.562Å at x=0 to 2.577 Å at x=0.1 in the IA–poor sample, while the $d_{(In–Se)4b}$ shortens from 2.672Å to 2.647Å gradually, see **Fig.2c**. This means that the difference (Δd) between $d_{(Ag–Se)4a}$ and $d_{(In–Se)4b}$ becomes smaller with the Zn content (x) increasing in the IA–poor sample, which suggests that the mixture of the longer $(Zn–Se)_{4a}$ bond with shorter Ag–Se bond results in an elongation in the bond length of 4*a*-Se, while the mixture of shorter $(Zn–Se)_{4b}$ and longer In–Se bond would shrink the crystal lattice. However, the things seem to be different in the Ag–poor samples. There are no tendency of change for both the $d_{(Ag–Se)4a}$ and $d_{(In–Se)4b}$ values with Zn content increasing, which makes the difference (Δd) between $d_{(Ag–Se)4a}$ and $d_{(In–Se)4b}$ remain almost constant with x increasing (see blue line and symbols) (**Fig.2c**). Such alterations of the structural parameters verify the fact that most Zn atoms occupy the cation sites in AIS, which is of great significance in scattering shortwave phonons.

Based on the Rietveld refinement results above, we therefore believe that the proposed defects Zn^{+1}_{Ag} (Zn^{-1}_{In}) from the band structure calculation should be directly related to the occupations of Zn in Ag(In)–poor AIS as Zn substitutes for Ag (In). It is the defect (Zn^{+1}_{Ag} or Zn^{-1}_{In}) that yield the "lowering" (or "lifting") of both the CBM and VBM simultaneously.

2.3 Thermoelectric Properties

Since the Fermi level tends to rise toward the conduction band upon the substitution of Zn for Ag, we believe that such a substitution, similar to the Zn substitution for Cu in $CuFeS_2$,[18] which has helped the occupation of Zn in the Ag site and form the donor defect Zn^{+1}_{Ag}, could generate more electrons in AIS. Meanwhile In–poor has a tendency to decrease the concentration of electrons upon the substitution of Zn for In because of the dominant role played by the acceptor Zn^{-1}_{In}. The changes in carrier concentration (n) can be verified by the measurements which reveal that the n values are ~$5\times10^{22}$$m^{-3}$ in In–AIS, ~$5\times10^{24}$$m^{-3}$ in Ag–poor and ~1×10^{24} m^{-3} in IA–poor at RT (**Table 3**). The magnitude of n value of the intrinsic $InAgSe_2$ at RT is almost the same order as what has been reported (4×10^{22}~$5\times10^{23}$$m^{-3}$).[11–13] The n value of In–poor is about 3~4 orders of magnitude smaller than the optimal one (10^{25} ~ 10^{26} m^{-3}),[10] and it is in good agreement with the change of the band structures. In addition, there is a small fluctuation in n value in the same series materials, probably because the solubility of Zn in AIS is limited (x<0.1), and more Zn content (x≥0.1) in Ag–poor and IA–poor does not help increase the carrier concentration n. That is why we observed the lowest n value at x=0.1 in Ag–poor compared to those at x=0.025 and 0.05.

Based on the above measured carrier concentration values, we disregard the In–poor, and center our work on Ag–poor and IA–poor in the following investigations.

Upon substitution of Zn for Ag and In simultaneously (IA–poor), the compounds still show n–type semiconductor behavior. The absolute α value at ~815K generally decreases with Zn content increasing from 291.1 (±16.2) at x=0.025 to 240.2 (±12.4) μV/ K at x=0.1 (**Fig.3a**), and the σ value increases from $3.6(\pm0.25)\times10^3$ to

5.7(±0.40)×10^3 Ω^{-1}m^{-1} (**Fig.3b**). In addition, we did not observe a systematic enhancement in κ_L in IA–poor with Zn content increasing from x=0.025 at low temperatures until 680K (**Fig.3c**), which might be due to the weak influence of crystal defects on κ_L upon Zn substitution for Ag and In simultaneously. For the sample at x=0.05 the κ_L value reduces from 0.69 (±0.11) WK^{-1}m^{-1} at near RT to 0.27 (±0.05) WK^{-1}m^{-1} at ~815K, and the highest ZT value is 0.95±0.10 at ~815K (**Fig.3d**). The total κ values are shown in the **Fig.S6**.

In IA–poor we did not observe the visible change of the bandgap (E_g~0.9eV) (**Fig.S7**). This is closely related to the reducing difference (Δd) between $d_{(Ag–Se)4a}$ and $d_{(In–Se)4b}$ (**Fig.2c**),[17] and to the fact that the effect of the antisite defects Zn^{+1}_{Ag} and that of Zn^{-1}_{In} neutralize. Hence the decreasing (increasing) in α (σ) in IA–poor is considered to be the sole enhancement of the carrier concentration n when Zn content increases. The enhancement in κ_L at x>0.025 is related to the reducing Δd and deviation from 0.25 of anion position displacement u,[23] which will further be discussed below.

The electrical properties of Ag–poor against temperature is plotted in **Fig.4a and b**. The absolute α value at ~815K decreases generally from 226.8 (±11.4) (x=0.025) to 195.5 (±9.8) μV/K (x=0.1) (**Fig.4a**), and an insert in **Fig.4a** is close–up view of the plots α (T) for the samples at x≥0.025, where the sample at x=0.1 whose carrier concentration is the lowest has the smallest Seebeck coefficient close to RT. The σ value at ~815K, which is much higher than that of IA–AIS, increases from 7.2(±0.5)×10^3 (x=0.025) to 1.1(±0.07)×10^4 Ω^{-1}m^{-1} (x=0.1) when Zn content increases (**Fig.4b**). The lattice thermal conductivity (κ_L) in Ag–poor reduces with the measuring temperature and Zn content. The sample at x=0.1 gives the lowest κ_L value that ranges from 0.38(±0.07)WK^{-1}m^{-1} at RT to 0.11(±0.02)WK^{-1}m^{-1} at 815K (**Fig.4c**), and the total κ is shown in **Fig.S8**. The highest ZT value is 1.05±0.12 at 815K (**Fig.4d**), which is about 3 times that of the intrinsic AIS. This material can be comparable to the state–of–the–art semiconductors with chalcopyrite structures,[24,25] and shows promise for applications in the intermediate temperatures.

The In–poor series samples show much higher absolute α values and low electrical conductivities over the measuring temperature region if compared to those of IA–poor and Ag–poor (see **Fig.S9 a** and **b**), which is mainly caused by the low carrier concentration n when Zn substitutes for In (see **Table 3**). At the meantime, they have relatively low κ and ZT values (ZT_{max}=0.33 for x=0.05 at 774K) (see **Fig.S9 c** and **d**) due to low electrical conductivities. Therefore, we center the discussion on the IA–poor and Ag–poor series materials.

The relatively low α and high σ values in Ag–poor are expected because the Fermi level tends to rise toward the conduction band upon Zn substitution for Ag, and results in an increase in the carrier concentration n. However, the experimentally determined bandgap in Ag–poor reveals that it tends to widen up a little (from ~0.9eV to ~0.97eV) when Zn content increases (shown in **Fig.S10**), which does not seem to be in agreement with the seeming improvement of the electrical conductivity. The origin for the E_g widening is, on one hand, due to the big difference (Δd) between $d_{(Ag–Se)4a}$ and $d_{(In–Se)4b}$ (**Fig.2c**) that leads to the relatively weakened hybridization (bonding) between Ag–d and Se–p near the bandgap region upon Zn substitution for Ag. Because in ternary chalcopyrite semiconductors the bandgap anomaly ΔE_g correlates nearly linearly with the existence of d bonding.[17, 26–28] On the other hand, the widening of E_g could be resulted from the increasing ionicity, which was proposed by Honeyman,[16] who found that energy gap increases with the crystalline ionicity. In this regard, we propose that the electrical property in Ag–poor is governed at least by two factors, which are the carrier concentration n and bandgap E_g. However, the positive effect from the increased n seems to be more prominent than the effect from the widening of E_g, which can be confirmed by the remarkable improvement in electrical conductivity (σ) and the decrease in Seebeck coefficient (α) upon the Zn substitution.

In addition, it is hard to quantitatively determine the effect of the minor impurity phase ($Zn_{0.4}In_2Se_{3.4}$) on α and σ values in the present work. However, in the same series materials with limited variation of carrier concentration n, presumably under the condition that the Ag–poor at x≥0.025 are degenerate semiconductors, then the α value should be mainly governed by the carrier concentration n and effective mass (m^*, according to the relation $\alpha \propto m^* n^{-2/3}$. In this case, it is possible that the Ag–poor sample (x=0.1) whose carrier concentration is the lowest has the smallest Seebeck coefficients at RT. Likewise, the σ value is determined by the two factors (carrier concentration n and mobility μ), the highest σ value at x=0.1 at high temperatures in the same series materials is mainly attributed to be high products of n and μ.

From the Rietveld refinements not only have we observed the displacement of the atomic Se (x_{Se}=0.2374 for AIS) upon Zn substitutions, but also reducing difference (Δd) between $d_{(Ag–Se)4a}$ and $d_{(In–Se)4b}$ in IA–poor (**Fig.2c**) that reduces the crystal distortion. Therefore, it is reasonable that the κ_L value increases with the Zn content increasing. While there still is a big difference between $d_{(Ag–Se)4a}$ and $d_{(In–Se)4b}$ in the Ag–poor, even though the difference (Δd) remains almost unchanged. That is way we observed the reduction in κ_L with the Zn content increasing. On the other hand, the anion position displacement (u), which is directly related to bond lengths (d_{AC} and d_{BC}) in ternary chalcopyrite semiconductors ABC_2,[27] can be estimated using the Abrahams–Bernstein rule.[29,30] However, we can not ignore the fact that the Abrahams–Bernstein rule is not a very accurate way to estimate the u values for $A\mathrm{In}C_2$, $\mathrm{Ag}BC_2$, and $\mathrm{ZnSn}C_2$ compounds with the chalcopyrite structure.[27] Hence a more reasonable method to estimate the anion displacement u in AIS–based semiconductors was proposed below,[27]

$$u = \frac{1}{4} + \frac{\beta - \left[\beta^2 - (2+\eta^2)\alpha^2\right]^{\frac{1}{2}}}{4\alpha} \qquad (10)$$

where α and β are defined by

$$\alpha = (r_A + r_c)^2 - (r_B + r_c)^2 \quad (11)$$

$$\beta = (r_A + r_c)^2 + (r_B + r_c)^2 \quad (12)$$

Here, r_A, r_B and r_C each represents the elemental radii of *A*, *B* and *C*. In the present material, $r_A(r^+_{Ag})$ =1.52Å, $r_B(r^{3+}_{In})$ =1.44Å and $r_c(r^{2-}_{Se})$ =1.14Å. According to **eqn.10**, we obtained the *u* value of 0.2611 for the intrinsic AIS, about 1.2~4.4% larger than the values (0.2500~0.2580) determined from Spiess etc.,[31-33] but smaller than the value (0.2700) determined by Abrahams–Bernstein rule. Although it is difficult to determine the *u* values when Zn (r^{3+}_{Zn} =1.31Å)[27] partially occupies the Ag and/or In sites according to the **eqn. 10, 11** and **12** as mentioned above, we predict based on **eqn. 10, 11** and **12** that the *u* value will rapidly drop from 0.2611 to –9.41 when Zn occupies all Ag sites in AIS, but increases from 0.2611 to 0.28 if Zn occupies all In sites. Of course, under such an extreme condition with Zn occupying in all Ag or In sites, a different substance that will invalidate the estimation of *u* value might form. In this sense, we believe, on one hand, that we are able to obtain a *u* value that is lower than 0.25 if only a small amount of Zn substitutes for Ag, and that *u* will be dramatically deviated from 0.25 if Zn content increases in Ag–poor. Such deviation will also reduce the lattice κ_L remarkably (see **Fig.4c**).[23] However, the case is different in IA–poor in terms of the above analysis. Because the anion displacement *u* upon substitution of Zn for In changes in an opposite way as it does upon Zn substitution for Ag, therefore, the deviation of the *u* value from 0.25 might become smaller with Zn content increasing in IA–poor. That is why we observed the gradual enhancement in κ_L in IA–poor with Zn content increasing from *x*=0.025 (**Fig.3c**). Of course, it is noteworthy that the minor phase $Zn_{0.4}In_2Se_{3.4}$ identified at *x*=0.1 (**Fig.S1**) might result in an inaccuracy in determining the constants *a* and *c* (**Fig.2a and b**). However, the possible error in *u* value generated by the precipitation of this minor phase should be much smaller than the change of *u* value by the anion displacement.[18] The grain boundaries in the precipitated minor phase $Zn_{0.4}In_2Se_{3.4}$ can scatter phonons, which yields an extra reduction in κ_L; but the reduction in κ_L caused by the phonon scattering on the extra grain boundaries is limited at high temperatures because the intrinsic AIS itself is a compound full of lattice defects.[26] The rapid increase in κ_L above ~675K for the sample IA–AIS at *x*=0.1 has proved this issue.

3. Experimental Section

Sample preparation Stoichiometric amounts of Ag, In, Zn and Se with 5N purity, according to the chemical formulas of $AgIn_{1-x}Zn_xSe_2$, $Ag_{1-x}InZn_xSe_2$, $Ag_{1-x}In_{1-x}Zn_{2x}Se_2$ (*x*=0, 0.025, 0.05, 0.1), were loaded into four different quartz tubes and then vacuum melted at 1373K for 24h, with a 30s rocking conducted every 1h to ensure homogenous composition without segregation. The melt was then cooled down slowly to 773K and annealed for 168h at this temperature, followed by a slow cooling procedure in furnace. The as–solidified ingots were pulverized and then ball–milled in stainless steel bowls that contain petroleum ether at a rotation rate of 350rpm for 5h. Subsequently, the dried powders were sintered by using spark plasma sintering apparatus (SPS–1030) with a designed sintering program under a pressure of 55MPa and at the highest temperature of 823K. The densities of the sintered samples were measured by using Archimedes' method. Each sample was cut into ~3mm slices measuring ~2.5 mm ×13 mm out of the sintered block, whose size is ϕ 20 mm × 2.5 mm, for electrical property measurements.

Physical property Measurements Electrical properties, including the Seebeck coefficient (α) and electrical conductivity (σ) as a function of temperature, were measured by using ULVAC ZEM–2 apparatus in helium atmosphere from RT to ~823 K, with errors of 7.0% and 10.0% on the absolute values of the Seebeck coefficient and electrical conductivity respectively. A temperature difference of around 5°C has been applied to two terminals of the sample to measure the Seebeck coefficient, whereas the electrical conductivity was measured by using the four–probe method. The thermal diffusivities were measured using TC–7000 and then checked using TC–1200RH. The heat capacities (C_p) were estimated through Debye model that is used for lattice vibronic energy, whose relation is as follows:[34]

$$C_p \sim C_v = 3nRF(\theta_D/T) \quad (13)$$

Here *n* is the number of atoms per formula unit, *R* is the gas constant, θ_D is the Debye temperature (θ_D= 191K for AIS),[35] and the Debye function $F(\theta_D/T)$ is defined by [35]

$$F(\theta_D/T) = (T/\theta_D)^3 \int_0^{\theta_D/T} \frac{3x^4 e^x}{(e^x-1)^2} dx \quad (14)$$

In the high temperature limit ($T \gg \theta_D$), $F(\theta_D/T)$ approaches to be unity (see **Fig.S11**), then the heat capacity (C_p) can roughly be estimated as $C_p \sim 3nR$, which is the well known Dulong–Petit's law. Thus, the thermal conductivities (κ) can be calculated as the products of material densities, thermal diffusivities and specific heats. However, the C_p values estimated based on the equation $C_p = 3nRF(\theta_D/T)$ are more often applied to gas, and can suffer a slight underestimation when it comes to a solid material especially at high temperatures. It is reported [25] that the underestimation using Dulong–Petit's equation could reach as high as ~3% at ~1000K. In this case the κ values would thus be a little underestimated and *ZT* values overestimated. The α, σ, κ three parameters were confirmed by taking the average values of three samples tested with the same method. The Hall coefficient (R_h) measurements at RT were conducted on a Hall effect measurement system (PPMS, Model–9) by using a four–probe configuration with a magnetic field sweeping between ±1.2 T and then performed on a 2×2×8 cm^3 rectangular samples. The Hall mobility (μ) and carrier concentration (*n*) were subsequently calculated based on the relations $\mu = -R_h \sigma$ and $n = -1/(e R_h)$ respectively, in which *e* is the electron charge. The current

and Hall voltage leads were fine copper wires, and the contacts were made of silver paste. Perkin–Elmer Lambda 950 UV–VIS–NIR spectrophotometer were used for the measurements of the absorption coefficient, and the absorption spectra of the powders were recorded between the visible and part of infrared regions (200 ~ 1200 nm).[36]

Structural and chemical compositions analysis The structural analysis of the powders was made by powder x–ray diffractometer (D8 Advance) operating at 50 kV and 40 mA. Cu Kα radiation (λ=0.15406 nm) and a scan rate of 4° min^{-1} were used to record the patterns ranging from 10° to 140°. The chemical compositions in $Ag_{1-x}InZn_xSe_2$ and $Ag_{1-x}In_{1-x}Zn_{2x}Se_2$ (x=0, 0.1) were analyzed by an electron probe micro–analyzer (EPMA) (S–4800, Hitachi, Japan) with accuracy > 97%.

Rietveld refinements using XRPD were performed using FULLPROF, and X-ray diffraction peakshapes were quantified by a Pseudo-Voigt function and a Pseudo-Voigt function with the Finger-Cox-Jephcoat asymmetry correction, respectively. The background was described as a shifted Chebyschev type. The following parameters were refined: lattice parameters, peak shape parameters, atomic coordinates, isotropic displacement parameters (U_{iso}) and site occupation factors (SOFs). The chalcopyrite $AgInSe_2$ was taken as a starting material, and each structural model was refined to convergence.

The attained crystal structure parameters in the present work, rather than the Boltzmann transport theory reported in ref. [37], were used to quantitatively explaine the transport properties.

Band structure calculations Plane–wave pseudopotential technique was applied to the calculation of the *ab inito* by using Cambridge Serial Total Energy Package (CASTEP) software [38] based on density functional theory (DFT). The generalized gradient approximation (GGA) [39] was used, and the Perdew–Burke–Ernzerhof (PBE) functional was adopted as the exchange-correlation energy. We used the norm conserving pseudopotential with a cutoff energy of 765eV and a k mesh of 4 × 4 × 5 in the first Brillouin zone. The $4d^{10}5s^1$, $5s^25p^1$, $3d^{10}4s^2$ and $4s^24p^4$ were each treated as valence states of Ag, In, Zn and Se. The doping conditions keep the same structure but arrange Zn in one Ag and/or one In lattice site respectively, each of which corresponds to the 50.0 at.% Zn occupation in Ag (50.0 at.%) and/or In (50.0 at.%) lattice sites. In order to specify the changes in the band structure, non–symmetry is imposed in the calculation. In the geometrical optimization, all forces on atoms are converged to less than 0.03eVÅ^{-1}. The maximum ionic displacement is confined within 1×10^{-3}Å and the total stress tensor is reduced to the order of 0.05GPa. The structure is fully relaxed before the electronic properties were calculated. The band structure of intrinsic AIS was calculated for comparison.

4. Conclusions

Based on the calculations of the band structures of Zn substituted $AgInSe_2$, we found that the Fermi level tends to move toward the conduction band when Zn substitutes for Ag and forms the active donor defect Zn^{+1}_{Ag}. We also noticed a significant decrease in concentration n when Zn substitution for In, which lowers the Fermi level toward the valence band because of the primarily formation of acceptor Zn^{-1}_{In}. The thermoelectric performance has been improved upon the substitutions of Zn for Ag and In simultaneously with the maximum ZT value reaching 0.95±0.10 at ~815K, solely due to the enhancement in carrier concentration n. However, a higher ZT value can also be obtained (1.05±0.12 at 815K) by substituting a proper amount of Zn for Ag through enhancing the carrier concentration n and reducing the lattice thermal conductivity via modifying the crystal structure. It also should be noted that the more prominent effect caused by carrier concentration n than that of the widening of bandgap E_g is another factor that contributes to the high ZT value.

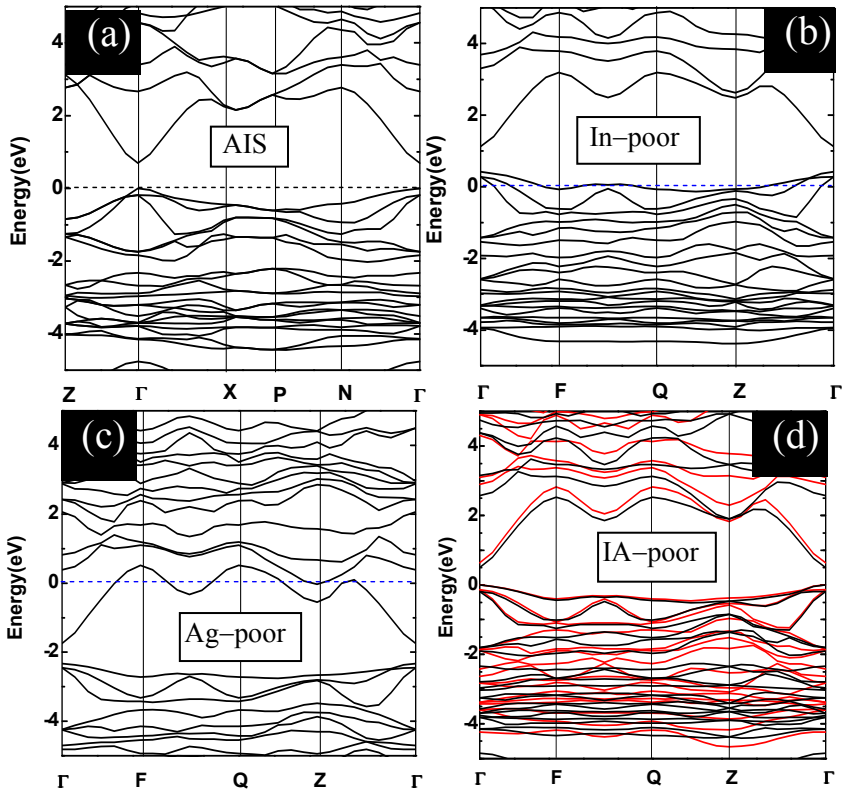

Fig.1 Calculated band structures (a) intrinsic $AgInSe_2$ (AIS), (b) Zn substitution for In (In–poor), (c) Zn substitution for Ag (Ag–poor) and (d) Zn substitution for In and Ag simultaneously in $AgInSe_2$ (IA–poor).

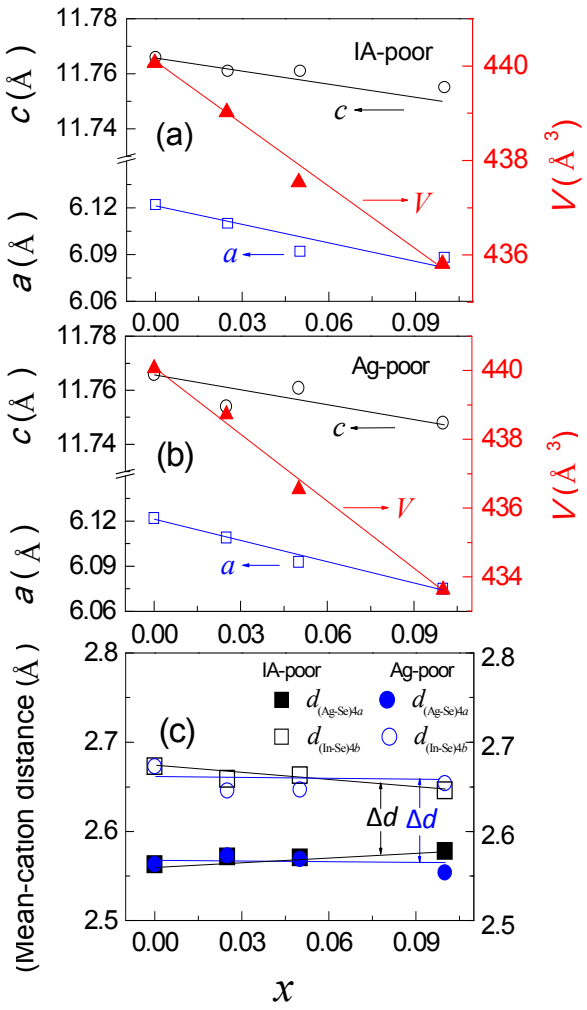

Fig.2 Zn content (x) versus lattice parameters (a, c), volume (V) for (a) IA–poor and (b) Ag–poor compounds, and Mean cation–Se distance (c) derived from Rietveld refinements using parameters shown in Table 1.

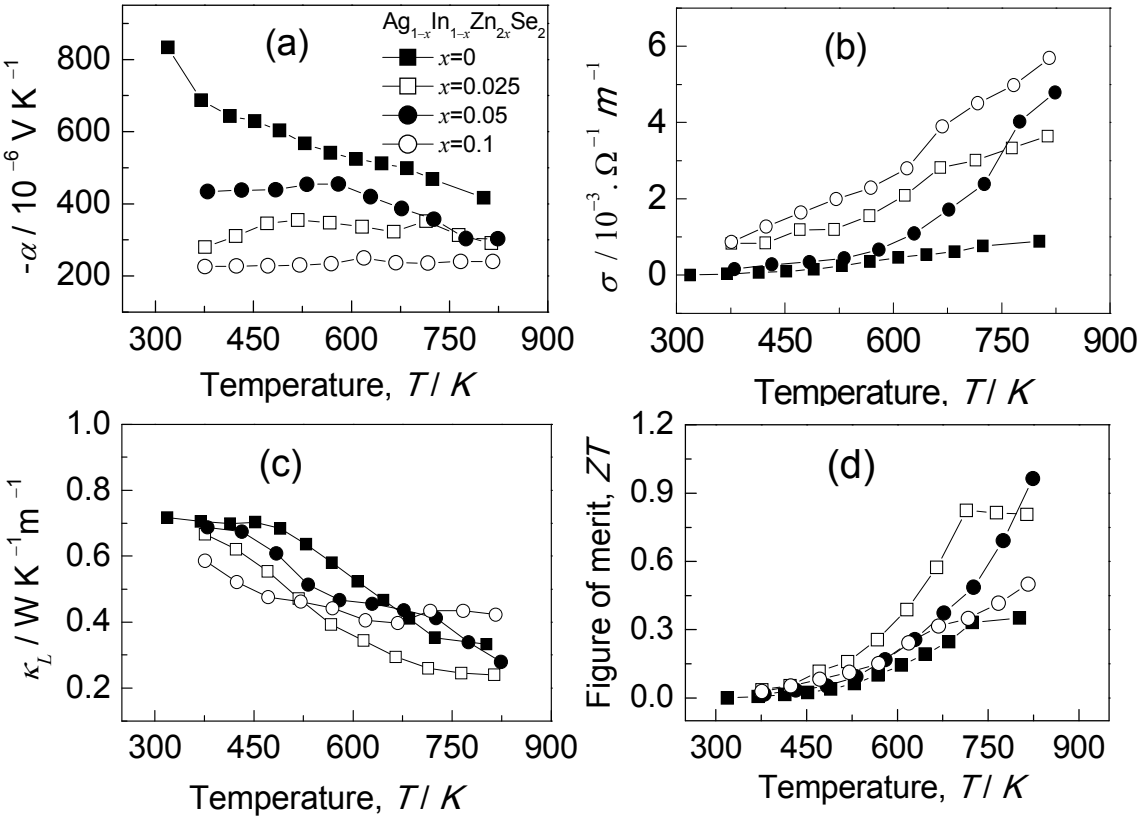

Fig.3 Thermoelectric properties of $Ag_{1-x}In_{1-x}Zn_{2x}Se_2$, (a) Seebeck coefficients (α), (b) electrical conductivities (σ), (c) lattice thermal conductivities (κ_L), (d) *ZT* values.

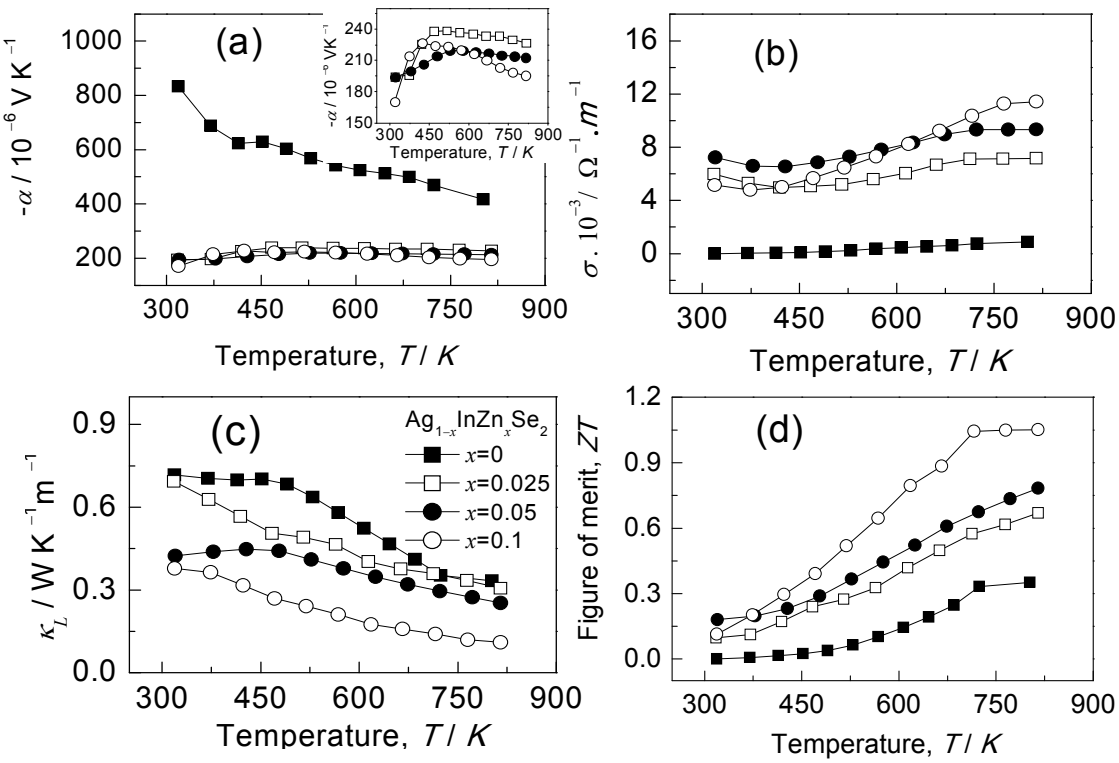

Fig.4 Thermoelectric properties of $Ag_{1-x}InZn_xSe_2$, (a) Seebeck coefficients (α), an insert is a magnified plot of α (T) for the samples with x≥0.025 (b) electrical conductivities (σ), (c) lattice thermal conductivities (κ_L), (d) ZT values.

Table 1 Structural parameters and refinement details for IA–poor compounds ($Ag_{1-x}In_{1-x}Zn_{2x}Se_2$) obtained by Rietveld refinements

Parameters	IA–poor	In–poor	Ag–poor
	Model A	Model A	Model A
	Cation 4*a*		
SOF(Ag)	0.9383(1)	0.9756(3)	0.9498(6)
SOF(Zn)	0.0479(3)	–0.0015(2)	0.0497(3)
SOF(In)	0.0001	0.0004(1)	0
100Uiso [Å^2]	1.9780(8)	1.9530(7)	2.0660(6)
	Cation 4*b*		
SOF(In)	0.9433(7)	0.9438(9)	0.9822(2)
SOF(Zn)	0.0495(5)	0.0480(8)	0.0011(2)
SOF(Ag)	0.0007(2)	0.0029(4)	0.0019(4)
100Uiso [Å^2]	2.3870(6)	2.2350(7)	2.4610(7)
	Anion 8*d*		
SOF(Se)	0.9490(1)	0.9944(5)	0.9833(4)
100Uiso [Å^2]	1.6050(6)	1.4110(3)	1.5750(8)
x_{Se}	0.2395(3)	0.2462(1)	0.2396(1)
	Reliability factors		
χ^2	1.5810	1.6860	1.6830
wR_p	0.0885	0.0970	0.0927
R_p	0.0703	0.0760	0.0736

Table 2 Lattice deformation parameters u and η for AIS, carrier concentrations n and mobility μ at RT of different compounds annealed for 168h at 773K.

Samples	x	Carrier concentration, n $[1/m^3]$	Mobility, μ $[cm^2V^{-1}s^{-1}]$	$\sigma[\Omega^{-1}m^{-1}]$	u	η
AIS	0	2.04×10^{23}	0.51	1.66	0.2611	0.9621
Ag–poor	0.025	5.12×10^{24}	73.05	0.60×10^{4}	N/A	
	0.05	6.68×10^{24}	67.33	0.72×10^{4}		
	0.1	4.96×10^{24}	64.95	0.52×10^{4}		
IA–poor	0.025	1.11×10^{24}	47.08	0.83×10^{3}		
	0.05	8.99×10^{23}	9.92	0.14×10^{3}		
	0.1	1.98×10^{24}	26.69	0.85×10^{3}		
In–poor	0.025	4.60×10^{22}	0.20	0.15		
	0.05	5.41×10^{22}	0.03	0.26×10^{-1}		
	0.1	4.40×10^{22}	0.04	0.29×10^{-1}		

Acknowledgements
This work is supported by the National Natural Science Foundation of China (51171084, 50871056), Zhejiang Provincial Natural Science Foundation (LY14E010003), and Ningbo International cooperation Project (2011D10012). We should also acknowledge the band structure calculation from Dr. H. Peng in Taiyuan University of Technology, Taiyuan, China

Notes and references

[a] Materials Science and Engineering College, China University of Mining and Technology, Xuzhou 221116, China.
[b] Institute of Materials Engineering, School of Materials, Ningbo University of Technology, Ningbo 315016, China.
[c] School of Chemistry & Environment, Beihang University, Beijing 100191, China.
†Corresponding author, J.L.Cui, E-mail: cuijiaolin@163.com
Electronic Supplementary Information (ESI) available: [Supporting Information is available from the RSC Online Library or from the author.]. See DOI: 10.1039/b000000x/

References

1 J.P.Heremans, V.Jovovic, E.S.Toberer, A.Saramat, K.Kurosaki, A.Charoenphakdee, S.Yamanaka and G. J.Snyder, *Science*, 2008, **321**, 554.
2 Y. Yan and J.A. Malen, *Energy Environ. Sci*., 2013,**6**, 1267.
3 C.M. Jaworski, B. Wiendlocha, V. Jovovic and J.P. Heremans, *Energy Environ. Sci*., 2011,**4**, 4155.
4 Y.Pei, X.Y.Shi, A.LaLonde, H.Wang, L.Chen and G. J.Snyder, Nature, 2011, **473**, 66.
5 H. Wang, Z.M. Gibbs, Y. Takagiwa and G. J. Snyder, *Energy Environ. Sci*., 2014,**7**, 804.
6 R.Venkatasubramanian, E.Siivola, T.Colpitts and B.O'Quinn, *Nature*, 2001, **413**, 597.
7 C. J.Vineis, A.Shakouri, A.Majumdar and M.G.Kanatzidis, *Adv. Mater*., 2010, **22**, 3970.
8 J.Rhyee, K. H.Lee, S.M.Lee, E.Cho, S. II Kim, E.Lee, Y.S.Kwon, J. H.Shim and G.Kotliar, *Nature*, 2009, **459**, 965.
9 H.L.Liu, X.Shi, F.Xu, L.Zhang, W.Zhang, L.Chen, Q.Li, C.Uher, T.Day and G.J.Snyder, *Nature Mater.*, 2012, **11**, 422.
10 G. J.Snyder and E. S.Toberer, *Nature Mater*., 2008, **7**, 105.
11 B.Tell, J.L.Shay and H.M.Kasper, *J. Appl. Phys*., 1972, **43**, 2469.
12 K.Yoshino, A.Kinoshita, Y.Shirahata, M.Oshima, K.Nomoto, T.Yoshitake, S.Ozaki and T.Ikari, *J. Phys.: Conf. Ser*., 2008, **100**, 042042.
13 B.Tell and H.M.Kasper, *J. Appl. Phys*., 1974, **45**, 5367.
14 P.Z.Ying, H.Zhou, Y.L.Gao, Y.Y.Li, Y.P.Li, X.L.Lian and J.L.Cui, *Key. Eng. Mater.,* 2012, **519**,188.
15 J. H.Schön, J.Oestreich, O.Schenker, H.Riazi-Nejad, M.Klenk, N.Fabre, E.Arushanov and E. Bucher, *Appl. Phys. Lett.*, 1999, **75**, 2969.
16 W. N.Honeyman and K. H.Wilkinson, *J. Phys. D: Appl. Phys.*, 1971, **4**, 1182.
17 S.Ozaki and S.Adachi, *J. Appl. Phys.*, 2006, **100**, 113526.
18 N. Tsujii and T. Mori, *Appl. Phys. Express* 2013, **6**, 043001.
19 J.L.Cui, Y.P.Li, Z.L.Du, Q.S.Meng and H.Zhou, *J. Mater.Chem.A*, 2013, **1**,677.
20 J. Yao, Z.Wang, J.V.Tol, N.S.Dalal and J.A. Aitken, *Chem. Mater*., 2010, **22**, 1647.
21 J. Yao, N.J.Takas, M.L.Schliefert, D.S. Paprocki, P. E. R. Blanchard, H. Gou, A. Mar, C.L.Exstrom, S.A. Darveau, P.F.P. Poudeu and J.A.Aitken, *Phys. Rev.B*, 2011, **84**, 075203.
22 S.M. Wasim, C. Rincón, J.M. Delgado and G. Marín, *J. Phys. Chem. Solids*, 2005, **66**, 1990.
23 W.C.Wu, Y.P.Li, Q.S.Meng, Z.Sun, W.Ren, J.F.Yang and J.L.Cui, *Appl. Phys. Lett*., 2013, **103**, 011905.
24 R.L.Liu, H.L.Xi, H.L.Liu, X.Shi, W.Q.Zhang and L.D.Chen, *Chem.Commun*., 2012, **48**, 3818.
25 T.Plirdpring, K.Kurosaki, A.Kosuga, T.Day, S.Firdosy, V.Ravi, G.J.Snyder A.Harnwunggmoung, T.Sugahara, Y.Ohishi, H.Mut and S.Yamanaka, *Adv. Mater*., 2012, **24**, 3622.
26 J.L.Shay, B.Tell, H.M.Kasper and L.M.Schiavone, *Phys. Rev. B*, 1973, **7**, 4485.
27 J.E.Jaffe and A.Zunger, *Phys Rev. B*, 1984, **29**, 1882.
28 J.L.Shay and H.M.Kasper, *Phys. Rev. Lett.*, 1972, **29**, 1162.
29 S.C.Abrahams and J.L.Bernstein, *J. Chem. Phys*., 1973, **59**, 5415.
30 S.C.Abrahams and J.L.Bernstein, *J. Chem. Phys*., 1974, **61**, 1140.
31 H.W.Spiess, V.Haeberln, G.Brandt, A.Rauber and J.Schncidcr, *Phys. Status Solidi B*, 1974, **62**, 183.
32 H.Hahn, G.Frank, W.Klingler, A.Meyer and G.Storger, *Z. Anorg. Allg. Chem*., 1953, **271**, 153.
33 P.Benoit, P.Charpin, R.Lesueur and C. Djaga-Mariadassou, *Jpn.J. Appl. Phys. Suppl*., 1980, **19–3**,85.
34 S. Adachi, *Properties of Group–IV, III–V and II–VI Semiconductors*, Ed: Wiley, Chichester, 2005.
35 J. B.Cáceres and C.Rincón, *Phys. Status Solidi B*, 2002, **234**, 541.
36 T.Colakoğlu and M.Parlak, *Appl. Surf. Sci.*, 2008, **254**,1569.
37 D.F. Zou, S.H. Xie, Y.Y. Liu, J.G. Lin and J.Y. Li, *J.Alloys Compds.* 2013, **570**, 150.
38 M. D.Segall, P. J. D.Lindan, M. J.Probert, C. J.Pickard, P. J.Hasnip, S. J.Clark and M. C.Payne, *J. Phys.: Condens. Mat*., 2002, **14**, 2717.
39 J. P.Perdew, K.Burke and M.Ernzerhof, *Phys. Rev. Lett*., 1996, **77**, 3865.

